Supplementary Information

Autonomous Nanomanufacturing of Lead-Free Metal Halide Perovskite Nanocrystals Using a Self-Driving Fluidic Lab

Sina Sadeghi,[a] Fazel Bateni,[a] Taekhoon Kim,[b] Dae Yong Son,[b], Jeffrey A. Bennett,[a] Negin Orouji,[a] Venkat S. Punati,[a] Christine Stark,[a] Teagan D. Cerra,[c] Rami Awad,[a] Fernando Delgado-Licona,[a] Jinge Xu,[a] Nikolai Mukhin,[a] Hannah Dickerson,[a] Kristofer G. Reyes[d] and Milad Abolhasani*[a]

[a] *Department of Chemical and Biomolecular Engineering, North Carolina State University, Raleigh, NC 27695, USA. Email: abolhasani@ncsu.edu*
[b] *Synthesis Technical Unit, Material Research Center, Samsung Advanced Institute of Technology, SEC, 130, Samsung-ro, Yeongtong-gu, Suwon-si, Gyeonggi-do, Republic of Korea.*
[c] *Department of Physics, Weber State University, Ogden, UT 84408, USA.*
[d] *Department of Materials Design and Innovation, University at Buffalo, Buffalo, NY 14260, USA.*

S1. Experimental Platform

Figure S1 presents the physical hardware of the developed self-driving fluidic lab (SDFL) for accelerated synthesis science studies of $Cs_3Cu_2I_5$ NCs. The experimental platform of the SDFL

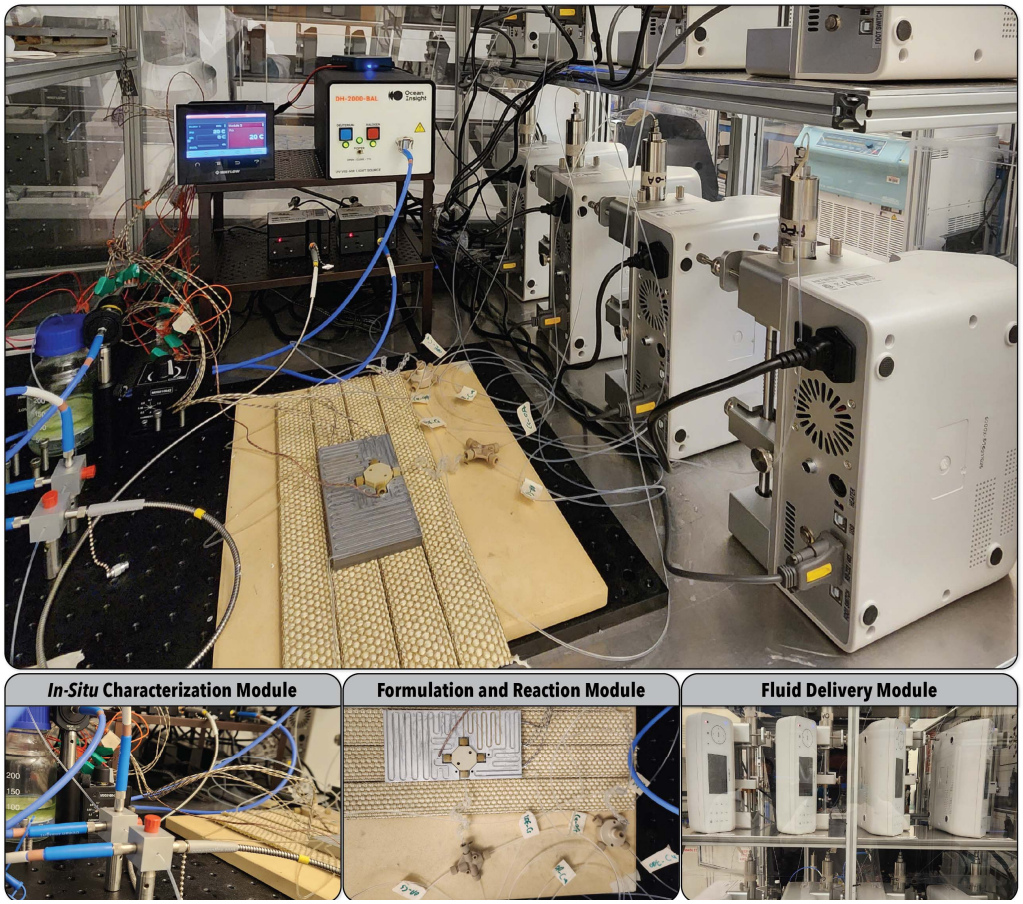

Figure S1. *Modular hardware of the developed SDFL, including the in-situ characterization, forumulation and reaction, and fluid delivery modules.*

includes three main modules: (i) fluid delivery, (ii) formulation and reaction, and (iii) *in-situ* characterization modules.

S2. Validation: *In-Situ* vs. *Ex-Situ* Spectroscopy

Figure S2 presents the UV-Vis absorption and and photoluminescence (PL) spectra of the in-flow synthesized $Cs_3Cu_2I_5$ NC sample obtained *in-situ*, using the two fiber-coupled spectrometers (HDX, Ocean Insight), compared against a bench-top balanced spectrometer (FS5, Edinburgh Instruments), demonstrating the accuracy of the *in-situ* characterization techniques utilized in the SDFL.

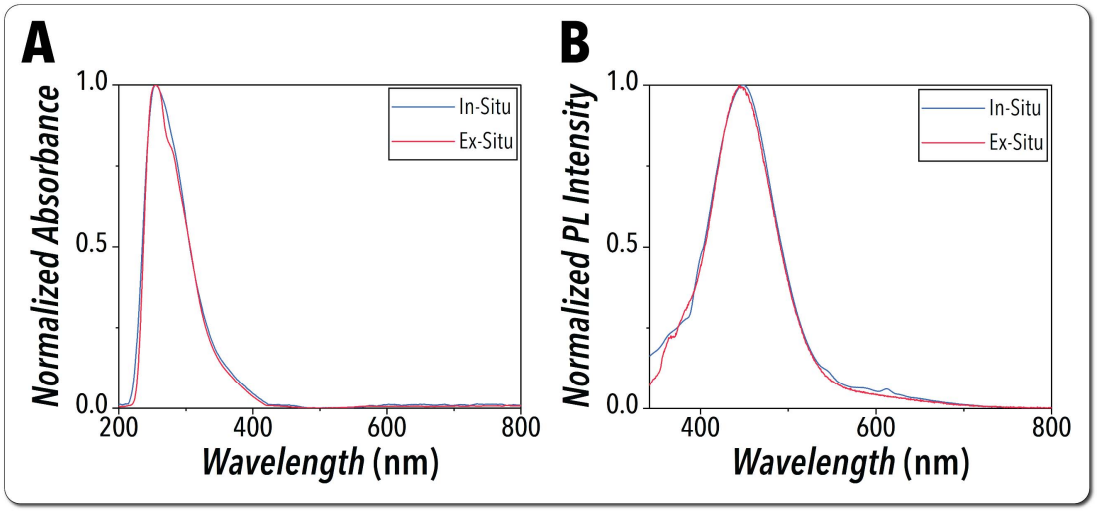

Figure S2. *Benchmarking of the optical spectra meassured in-situ using the fiber-coupled spectrometers vs. a bench-top spectrometer with the same in-flow synthesized $Cs_3C_2I_5$ NC sample: UV-Vis A) Absorption and B) PL.*

S3. Output Parameters: Optical Features of Interest

Figure S3 presents the linear correlation of *in-situ* measured NCs emission peak intensity (PL_I) *vs.* offline measured absolute photoluminescence quantum yield (PLQY) (FS5, Edinburgh Instruments). The *in-situ* obtained PL_I was utilized as a PLQY proxy in autonomous experimentation campaigns.

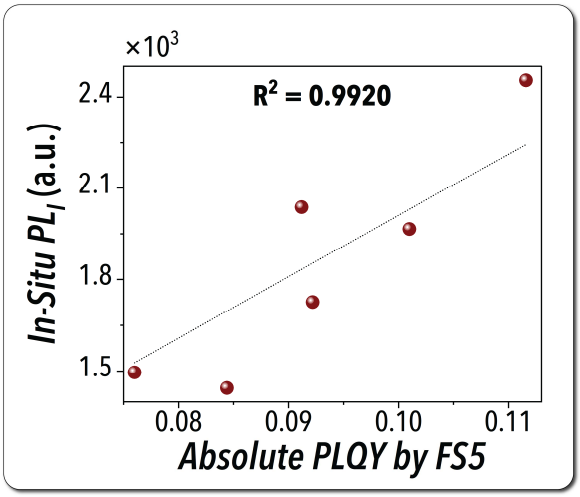

Figure S3. *Linear correlation of in-situ measured PL_I of the in-flow synthesized $Cs_3C_2I_5$ NC vs. offline measured absolute PLQY.*

S4. Process Automation

We developed a custom LabVIEW code to automatically control the hardware operation of the SDFL. The developed process automation module was paired with a custom-built Python script to not only execute experimental conditions but also analyze/process the *in-situ* obtained UV-Vis absorption and PL spectra of the as-synthesized $Cs_3Cu_2I_5$ NCs. The process automation operating interface is demosntrated in **Figure S4A**. A CSV file was parsed to the the LabView script to automatically access the experimental input parameters, including the precursors and carrier phase volumetric flowrates, reaction temperature, and equilibrium time (as a multiplier of the total residence time, discussed in the main text). Once the input parameters were read by the LabVIEW script, the process automation code had a waiting period for the reaction module of the SDFL to reach the set reaction temperature ± 1°C and to remain in that range for at least 1 min. **Figure S4B** shows the rates at which the reactor heating and cooling occured within the entire temperature range considered for autonomous experimentations in this study (120°C - 150°C). The characteristic cooling and hearing times required to achieve the largest temperature change accessible in this work by the SDFL were 6 min and 3 min, respectively. Following the temperature equilibration of the reactor plate, the process automation module of the SDFL initated the operation of the syringe pumps at their specified volumetric flowrates. Once the two-phase flow reached steady state operation (defined by the multiple of residence times discussed in the main text), the process automation module of the SDFL initated data acquisition *via* the *in-situ* characterization

module. An integration time of 40 ms was utilized to record 500 UV-Vis absorption and PL spectra of $Cs_3Cu_2I_5$ NCs for each experimental condition. Since no washing cycle was required due to the use of perfluorinated oil (PFO) as the inert carrier phase, the next set of input parameters was immediately parsed to the SDFL hardware for automatic testing. In the autonomous operation mode of the SDFL, once the UV-Vis absorption and PL spectra of the in-flow syntehsized $Cs_3Cu_2I_5$ NCs were recorded, the Python script proceeded with analyzing/processing the optical spectra to feed the processed data to the surrogate model of the Bayesian optimization (BO) algorithm for autoamtic selection of the new set of experimental condition(s) to be automatically performed by the SDFL hardware.

The data processing code implemented in Python was utilized to automatically obtain the optical features of interest from the *in-situ* obtained UV-Vis absorption and PL spectra of $Cs_3Cu_2I_5$ NCs. The UV-Vis absorption spectra of a specific experimental condition was obtained using the Beer-Lambert law and processing 500 *in-situ* obtained raw spectra as well as the previously aqcuired dark and solvent references. Next, the top 50 spectra with the highest absorbance values at the excitation wavelength of 300 nm ($Abs_{300\ nm}$) were averaged to ensure that the UV-Vis absoprtion spectra was obtained from the center of the reactive droplets passing through the *in-situ* characterization module of the SDFL. The processed PL spectra of $Cs_3Cu_2I_5$ NCs associated with a specific experimental condition was automatically obtained using a similar approach. The previously recorded dark reference was first subtracted from the 500 *in-situ* obtained raw PL spectra, and the top 50 with the highest PL_I values were then averaged to achieve the PL spectra corresponding to the reactive phase. The processed UV-Vis absorption and PL spectra of $Cs_3Cu_2I_5$ NCs were then utilized to automatically obtain the optical features of interest for subsequent machine learning (ML) modeling and experiment-selection. The optical features of interest include $Abs_{300\ nm}$, PL_I, and emission peak area (PL_A) of the in-flow synthesized $Cs_3Cu_2I_5$ NCs. Among the optical features, PL_I was utilized as the output parameter of interest for autonomous explorative and optimization campaigns. The data processing and BO codes can be accessed *via* our group's GitHub page: https://github.com/AbolhasaniLab

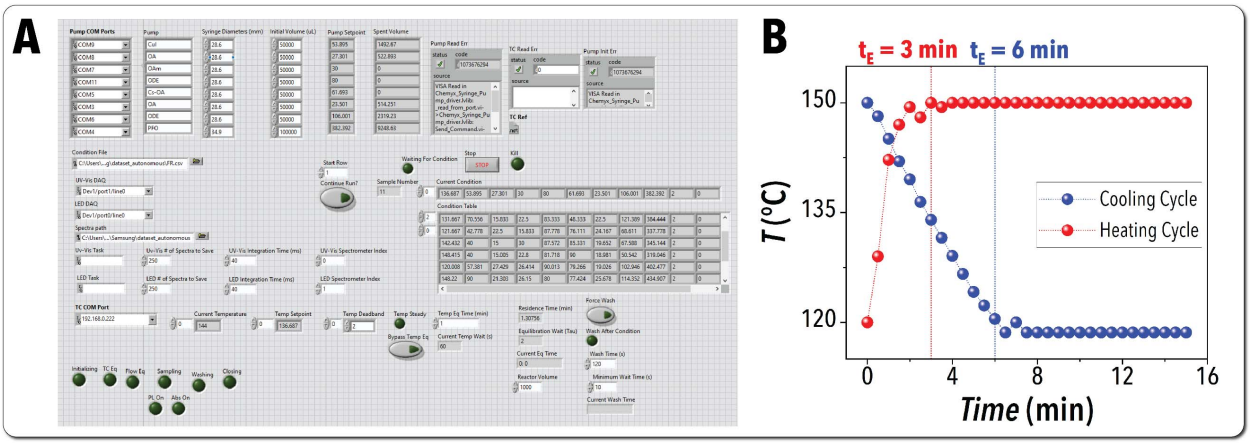

Figure S4. *A) The user interface snaphsot of the developed LabVIEW code for process operation of the SDFL. B) Reaction module heating and cooling rates within the entire temperature range considered for autonomous experimentation campaigns (120°C - 150°C).*

S5. Dynamic Residence Time Study

Figure S5 presents the values of PL_I and PL_A of the in-flow synthesized $Cs_3Cu_2I_5$ NCs asscoiated with the dynamic residence time study presented in the main manuscript.

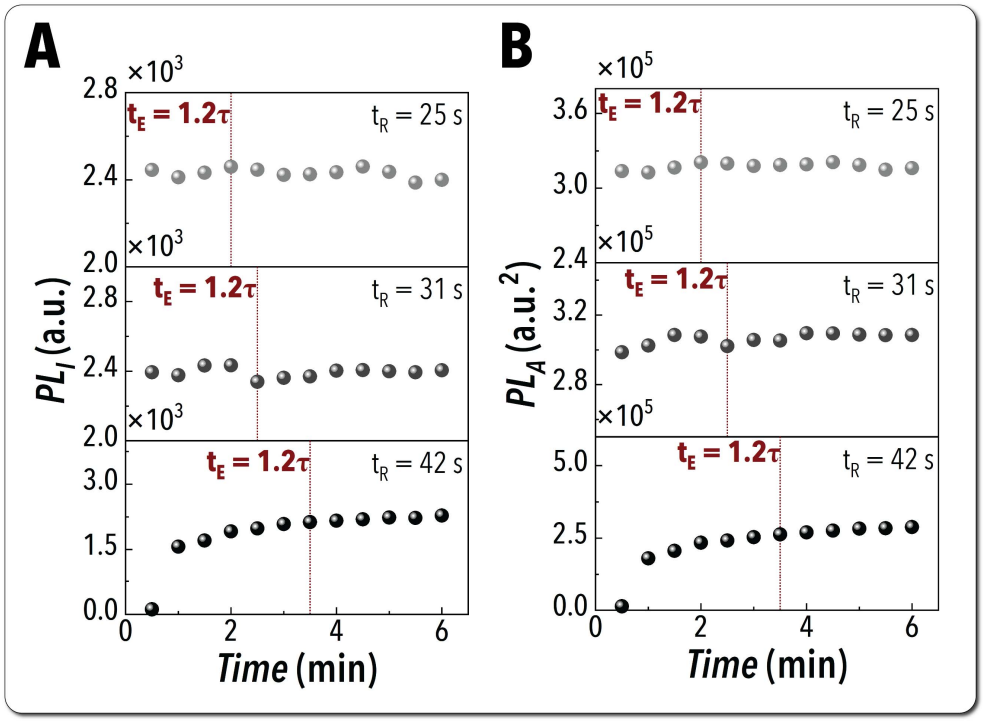

Figure S5. *The in-situ obtained optical features associated with three different reaction times utilized to examine the effect of dynamic residence time on the equilibrium time needed to initiate the in-situ characterization: A) PL_I and B) PL_A.*

S6. Effect of Reaction Time on Optical Properties of the In-Flow Synthesized NCs

Figure S6 presents the effcet of reaction time (12 s - 42 s) on the optical properties of the as-synthesized $Cs_3Cu_2I_5$ NCs. Increasing the reaction time up to 21 s increased the concentration of the NCs. However, the concentration of the in-flow synthesized $Cs_3Cu_2I_5$ NCs reached a plateu at reaction times higher than 21 s. In addition, the PL intensity of the NCs increased up to 28 s reaction time. Since the NCs PL_I was considered as a proxy for PLQY in this study, the reaction time interval of 25 s to 42 s was utilized for autonomous experimentation campaigns.

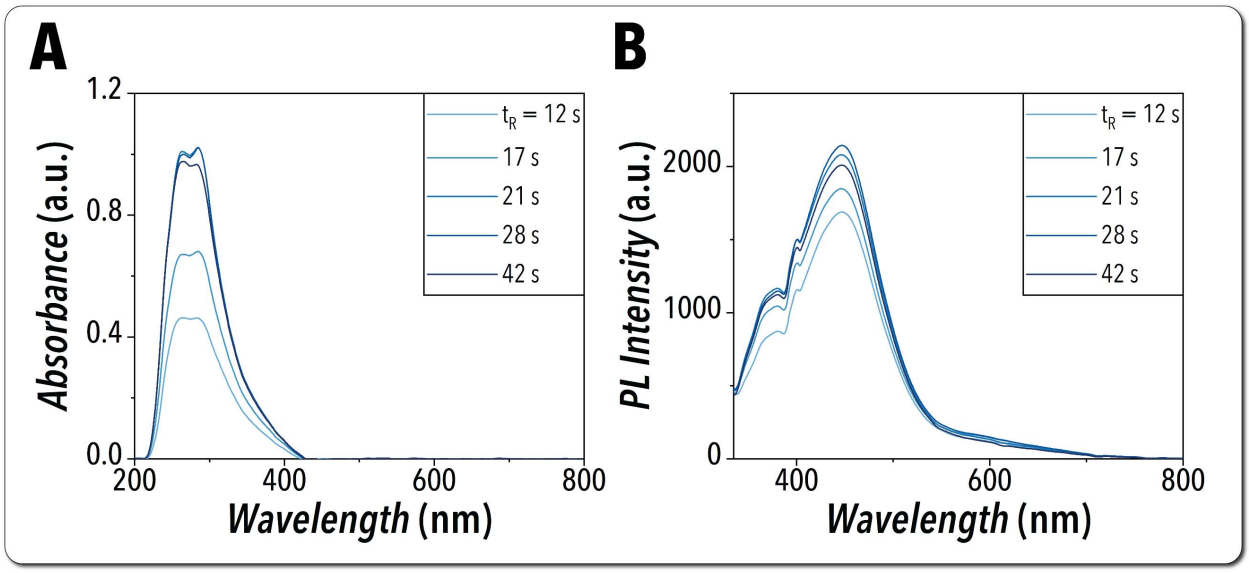

Figure S6. *In-flow study of the effect of reaction time on the optical features of $Cs_3Cu_2I_5$ NCs. In-situ recorded UV-Vis A) absorption and B) PL spectra of $Cs_3Cu_2I_5$ NCs at total flowrates above 600 µL/min to ensure mass transfer-indepedency of the formed NCs while maintaining the other synthesis input parameters constant ([CsOleate] = 12.00 mM, [CuI] = 4.00 mM, $[OA_{CsOleate}]$ = 161.00 mM, $[OA_{CuI}]$ = 151.40 mM, $[OAm_{CuI}]$ = 145.13 mM, T = 130°C).*

S7. Partial Grid Search

Figure S7 shows the complete *in-situ* obtained UV-Vis absorption spectra of $Cs_3Cu_2I_5$ NCs associated with the partial grid search study presented in the main text.

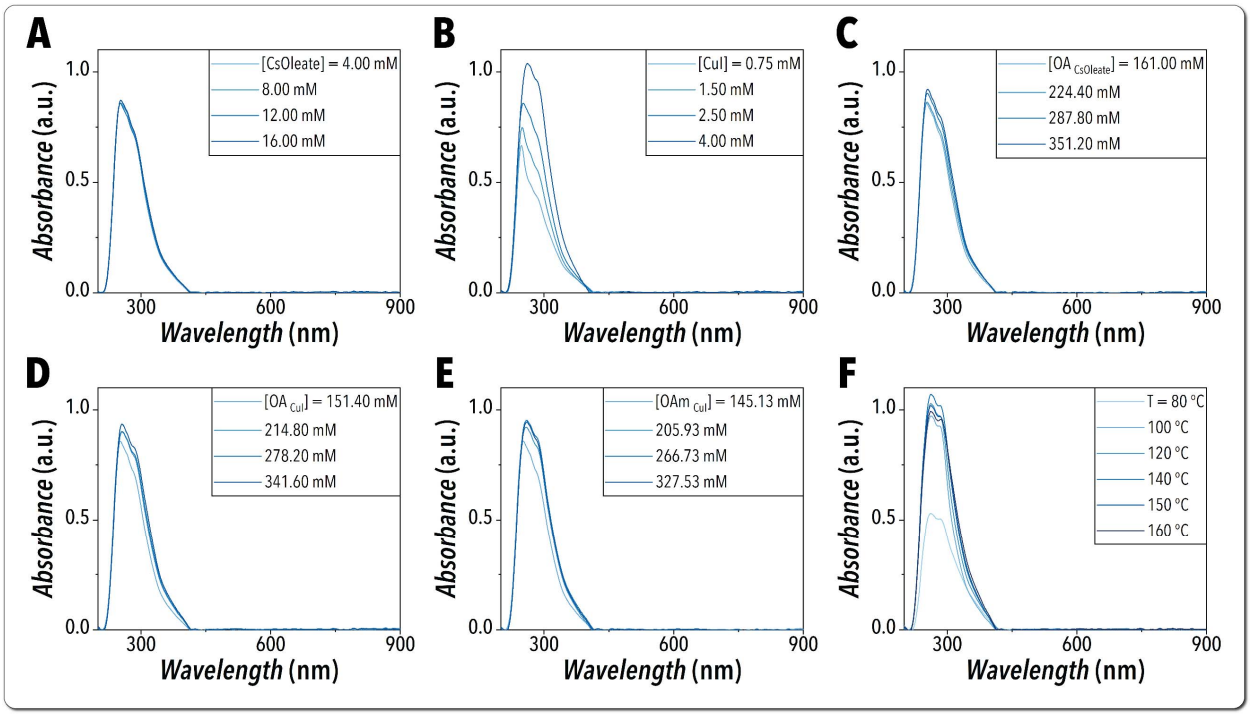

Figure S7. . *In-situ recorded UV-Vis absorption spectra of the partial grid search on the input synthesis parameters, including A) [CsOleate], B) [CuI], C) [$OA_{CsOleate}$], D) [OA_{CuI}], E) [OAm_{CuI}], and F) reaction temperature, while maintaining the reaction time constant.*

Table S1. *Summary of the experimental conditions conducted in the partial grid search study.*

Exp. #	Temp. (°C)	CuI ($\mu L.min^{-1}$)	OA_{CuI} ($\mu L.min^{-1}$)	OAm_{CuI} ($\mu L.min^{-1}$)	ODE_{CuI} ($\mu L.min^{-1}$)	CsOleate ($\mu L.min^{-1}$)	$OA_{CsOleate}$ ($\mu L.min^{-1}$)	$ODE_{CsOleate}$ ($\mu L.min^{-1}$)	PFO ($\mu L.min^{-1}$)
CsOleate-1	150.0	50.0	15.0	15.0	70.0	20.0	15.0	115.0	300.0
CsOleate-2	150.0	50.0	15.0	15.0	70.0	40.0	15.0	95.0	300.0
CsOleate-3	150.0	50.0	15.0	15.0	70.0	60.0	15.0	75.0	300.0
CsOleate-4	150.0	50.0	15.0	15.0	70.0	80.0	15.0	55.0	300.0
CuI-1	150.0	15.0	15.0	15.0	105.0	60.0	15.0	75.0	300.0
CuI-2	150.0	30.0	15.0	15.0	90.0	60.0	15.0	75.0	300.0
CuI-3	150.0	50.0	15.0	15.0	70.0	60.0	15.0	75.0	300.0
CuI-4	150.0	80.0	15.0	15.0	40.0	60.0	15.0	75.0	300.0
$OA_{CsOleate}$-1	150.0	50.0	15.0	15.0	70.0	60.0	15.0	75.0	300.0
$OA_{CsOleate}$-2	150.0	50.0	15.0	15.0	70.0	60.0	30.0	60.0	300.0

$OA_{CsOleate}$-3	150.0	50.0	15.0	15.0	70.0	60.0	45.0	45.0	300.0
$OA_{CsOleate}$-4	150.0	50.0	15.0	15.0	70.0	60.0	60.0	30.0	300.0
OA_{CuI}-1	150.0	50.0	15.0	15.0	70.0	60.0	15.0	75.0	300.0
OA_{CuI}-2	150.0	50.0	30.0	15.0	55.0	60.0	15.0	75.0	300.0
OA_{CuI}-3	150.0	50.0	45.0	15.0	40.0	60.0	15.0	75.0	300.0
OA_{CuI}-4	150.0	50.0	60.0	15.0	25.0	60.0	15.0	75.0	300.0
OAm_{CuI}-1	150.0	50.0	15.0	15.0	70.0	60.0	15.0	75.0	300.0
OAm_{CuI}-2	150.0	50.0	15.0	30.0	55.0	60.0	15.0	75.0	300.0
OAm_{CuI}-3	150.0	50.0	15.0	45.0	40.0	60.0	15.0	75.0	300.0
OAm_{CuI}-4	150.0	50.0	15.0	60.0	25.0	60.0	15.0	75.0	300.0
T-1	80.0	80.0	15.0	15.0	40.0	80.0	15.0	55.0	300.0
T-2	100.0	80.0	15.0	15.0	40.0	80.0	15.0	55.0	300.0
T-3	120.0	80.0	15.0	15.0	40.0	80.0	15.0	55.0	300.0
T-4	140.0	80.0	15.0	15.0	40.0	80.0	15.0	55.0	300.0
T-5	150.0	80.0	15.0	15.0	40.0	80.0	15.0	55.0	300.0
T-6	160.0	80.0	15.0	15.0	40.0	80.0	15.0	55.0	300.0

S8. Autonomous Experimentation

S8.1 Surrogate Model. We employed an ensemble neural network (ENN), including 20 cascade forward neural network (NN) models with randomized structures (6 to 8 hidden layers each including 15 to 30 nodes) to map seven independent input synthesis parameters (X_i, i:1-7) to one output parameter (*in-situ* measured PL_I of the in-flow synthesized $Cs_3Cu_2I_5$ NCs). A seed number of 100 was utilized to split the dataset into training/test sets (with an split ration of 80/20) and to randomize the ENN structure. The *RMSprop* optimizer with a learning rate of 10^{-4} and a maximum epoch number of 1000 was utilized in the model training stage. To combat overfitting, the Early-Stopping technique was employed with a patience of 50 and a min_delta of 10^{-5}.

S8.2 Input Synthesis and Output Parameters. The independent/dependent input synthesis and output parameters of the SDFL are as follows:

$$X_{1,T} = \frac{T-120}{150-120} \quad \text{(S1)}$$

$$X_{2,CuI} = \frac{Q_{CuI}-40}{90-40} \quad \text{(S2)}$$

$$X_{3,OA_{CuI}} = \frac{Q_{OA_{CuI}}-15}{30-15} \quad \text{(S3)}$$

$$X_{4,OAm_{CuI}} = \frac{Q_{OAm_{CuI}}-15}{30-15} \quad \text{(S4)}$$

$$X_{5,ODE_{CuI}} = \frac{Q_{ODE_{CuI}} - 80}{100 - 80} \quad \text{(S5)}$$

$$X_{6,CsOleate} = \frac{Q_{CsOleate} - 40}{90 - 40} \quad \text{(S6)}$$

$$X_{7,OA_{CsOleate}} = \frac{Q_{OA_{CsOleate}} - 15}{30 - 15} \quad \text{(S7)}$$

$$Q_{ODE_{CsOleate}} = Q_{CuI} + Q_{OA_{CuI}} + Q_{OAm_{CuI}} + Q_{ODE_{CuI}} - Q_{CsOleate} - Q_{OA_{CsOleate}} \quad \text{(S8)}$$

$$Q_{PFO} = Q_{CuI} + Q_{OA_{CuI}} + Q_{OAm_{CuI}} + Q_{ODE_{CuI}} + Q_{CsOleate} + Q_{OA_{CsOleate}} + Q_{ODE_{CsOleate}} \quad \text{(S9)}$$

$$\overline{PL_I} = \frac{PL_I}{5000} \quad \text{(S10)}$$

Here, X represents the independent dimensionless input parameter while T and Q represent the reaction temperature and precursor volumetric flowrate, respectively. **Equations S1 - S7** represent the dimensionless equations employed to achieve the input parameters used for the ML modeling, **Equations S8** and **S9** represent the dependent input synthesis parameters, and **Equation S10** represents the output parameter of interest used in autonomous experimentation campagins.

S8.3 Autonomous Experimental Campaigns. In this work, we utilized BO for autonomous synthesis science studies of $Cs_3Cu_2I_5$ NCs with the SDFL. The explorative campaign to build a digital twin model of the NC synthesis process was implemented using the maximum variance (MV) decision-making policy whereas expected improvement (EI), exploitation (EPLT), and upper confidence bound (UCB) experiment-selection policies were utilized for optimization campaigns. The objective function used in autonomous campaigns, $z(X)$, is defined as follows:

$$z(X) = |1 - \overline{PL_I}| \quad \text{(S11)}$$

Herein, the maximum PL_I of the in-flow synthesized $Cs_3Cu_2I_5$ NCs (5000 a.u.) achievable considering the output power of the 300 nm UV LED light source, used in the *in-situ* characterization module, was considered while formulating the objective function.

In each experimental iteration associated with a specific decision-making policy, we first passed the normalized PL_I values predicted by the ENN to the objective function and then employed the decision policy acquisition function[1] to achieve a scalar function. We subsequently utilized the *SLSQP* optimizer to minimize the scalar function and identify the corresponding input parameters. The extracted independent input parameters were then utilized to calculate the dependent parameters to achieve a complete set of input synthesis parameters for the next experiment(s) of the SDFL. The new BO-predicted experimental condition was subsequently

written to the CSV file read by the LabVIEW script of the SDFL to be automatically tested next. The developed BO codes can be accessed *via* our group's GitHub page: https://github.com/AbolhasaniLab

S9. NC Purification and *Ex-Situ* Characterization

The crude NC solutions collected from the outlet of the microfluidic reactor was first separated from the carrier phase (PFO) by gravitational separation and then centrifuged at 7000 rpm for 5 min. The supernatant was discarded, and precipitates were redispersed in hexane. The purified $Cs_3Cu_2I_5$ NCs were then characterized using transmission electron microscopy (TEM) imaging and X-ray diffraction (XRD) analysis. To study the morphology of the in-flow synthesized $Cs_3Cu_2I_5$ NCs, an FEI Talos F200X (200 kV) was utilized. To study the crystalline structure of the in-flow synthesized $Cs_3Cu_2I_5$ NCs, we utilized a Rigaku SmartLab X-ray diffractometer with Cu Ka radiation (λ = 0.154 nm) at a voltage of 40 kV.

Figure S8 presents the effect of reaction temperature on the $Cs_3Cu_2I_5$ NCs morphology and average size. **Figure S9** presents a TEM image of the highest-performing $Cs_3Cu_2I_5$ NCs autonomously discovered by the SDFL using the EI decision-making policy.

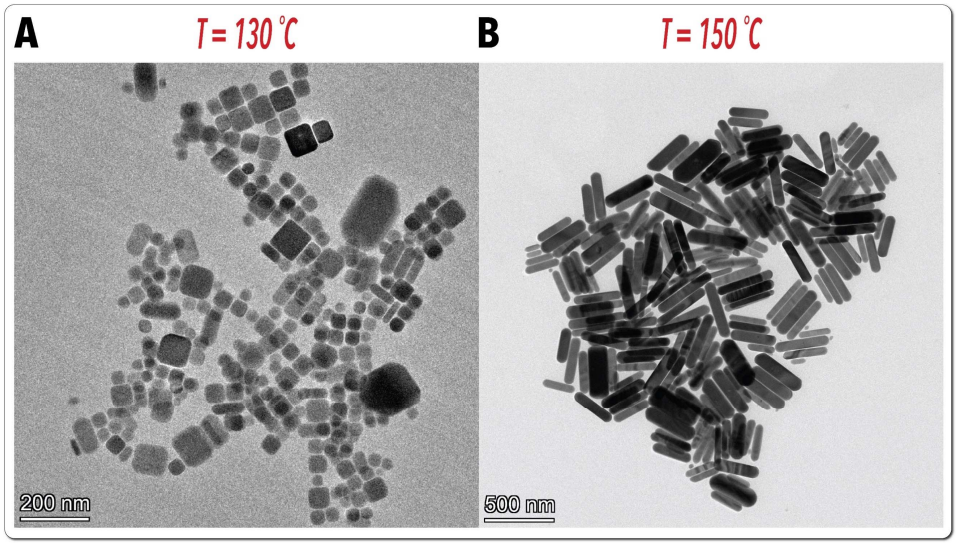

Figure S8. *TEM images associated with two $Cs_3Cu_2I_5$ NC samples synthesized in the microfluidic platform of the SDFL at two different reaction temperatures, A) 130°C and B) 150°C, while maintaining the other synthesis input parameters constant ([CsOleate] = 12.00 mM, [CuI] = 4.00 mM, [$OA_{CsOleate}$] = 161.00 mM, [OA_{CuI}] = 151.40 mM, [OAm_{CuI}] = 145.13 mM, t_R = 30 s).*

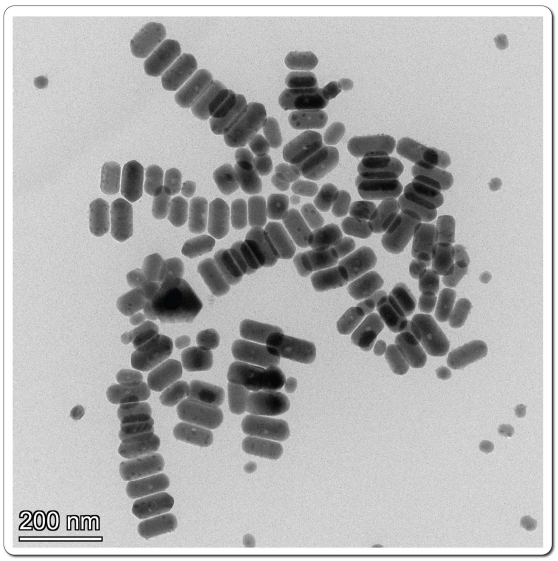

Figure S9. *TEM image of the highest-performing $Cs_3Cu_2I_5$ NCs autonomously synthesized by the developed SDFL using the EI decision-making policy.*

Table S2. *Summary of the experimental conditions conducted in the autonomous explorative campaign.*

Exp. #	Temp. (°C)	CuI ($\mu L.min^{-1}$)	OA_{CuI} ($\mu L.min^{-1}$)	OAm_{CuI} ($\mu L.min^{-1}$)	ODE_{CuI} ($\mu L.min^{-1}$)	CsOleate ($\mu L.min^{-1}$)	$OA_{CsOleate}$ ($\mu L.min^{-1}$)	$ODE_{CsOleate}$ ($\mu L.min^{-1}$)	PFO ($\mu L.min^{-1}$)	Normalized PL_I
1	141.7	65.0	29.2	24.2	92.2	42.8	17.5	150.3	421.1	0.340
2	128.3	87.2	24.2	17.5	81.1	87.2	19.2	103.6	420.0	0.206
3	131.7	70.6	15.8	22.5	83.3	48.3	22.5	121.4	384.4	0.366
4	121.7	42.8	22.5	15.8	87.8	76.1	24.2	68.6	337.8	0.295
5	125.0	76.1	17.5	25.8	96.7	53.9	15.8	146.4	432.2	0.454
6	135.0	59.4	20.8	29.2	85.6	81.7	27.5	85.8	390.0	0.395
7	138.3	48.3	27.5	27.5	98.9	65.0	25.8	111.4	404.4	0.294
8	145.0	81.7	25.8	20.8	90.0	70.6	29.2	118.6	436.7	0.595
9	148.3	53.9	19.2	19.2	94.4	59.4	20.8	106.4	373.3	0.521
10	120.0	81.8	27.5	29.2	95.5	84.5	19.1	130.4	468.0	0.482
11	122.9	52.5	24.7	30.0	80.0	52.0	15.0	120.2	374.5	0.379
12	120.0	61.8	22.7	30.0	88.8	49.5	26.7	127.1	406.7	0.396
13	147.1	41.8	20.4	30.0	80.0	56.5	29.7	86.0	344.5	0.322
14	145.0	40.0	15.0	26.8	100.0	78.3	28.0	75.5	363.6	0.318
15	148.0	40.0	24.6	15.0	90.8	89.8	22.4	58.1	340.8	0.404
16	121.7	82.0	16.1	21.4	81.3	46.4	29.6	124.7	401.5	0.597
17	147.7	69.0	20.0	15.0	87.2	84.6	15.0	91.6	382.3	0.585
18	135.2	58.6	23.0	19.3	98.6	87.9	15.3	96.4	399.1	0.513
19	145.0	54.8	28.7	24.2	92.4	78.2	15.0	106.9	400.1	0.481

20	144.1	86.6	15.9	23.8	86.0	79.6	15.0	117.7	424.5	0.624
21	149.4	40.0	29.1	29.8	93.8	90.0	15.0	87.7	385.4	0.341
22	144.9	85.9	25.4	15.0	98.4	62.3	30.0	132.5	449.6	0.592
23	145.1	83.0	27.1	18.2	91.7	40.0	27.3	152.6	439.9	0.573
24	120.0	75.7	21.4	15.0	92.6	57.5	27.6	119.6	409.3	0.558
25	145.3	40.9	29.9	26.3	93.4	48.8	21.0	120.8	381.1	0.348
26	142.0	89.3	30.0	15.0	80.0	40.0	21.7	152.6	428.5	0.589
27	146.9	73.7	15.0	28.2	83.3	40.0	15.0	145.2	400.5	0.580
28	125.5	76.2	15.0	23.1	96.3	40.0	16.4	154.3	421.3	0.563
29	150.0	55.8	15.0	15.0	100.0	40.0	22.4	123.4	371.5	0.514
30	121.7	40.0	27.2	16.4	94.7	40.0	25.6	112.8	356.8	0.334
31	142.6	66.6	27.0	15.0	96.4	54.5	15.0	135.5	410.1	0.539
32	120.0	82.3	30.0	15.0	80.0	40.0	30.0	137.3	414.7	0.555
33	150.0	77.8	26.7	20.5	80.0	67.6	28.2	109.2	410.1	0.604
34	120.0	90.0	24.6	29.6	95.2	40.0	22.6	176.8	478.7	0.572
35	137.8	66.5	15.0	25.5	80.0	88.9	23.9	74.1	373.9	0.563
36	133.7	82.2	15.9	16.1	92.0	75.6	29.0	101.7	412.4	0.619
37	142.8	41.1	15.0	15.0	96.7	85.5	25.9	56.3	335.7	0.453
38	120.0	55.1	25.5	22.3	96.4	54.9	15.0	129.4	398.6	0.445
39	120.0	83.0	15.5	19.1	95.3	90.0	15.0	107.9	425.7	0.570
40	120.0	90.0	15.0	17.8	89.6	40.0	15.0	157.5	425.0	0.629
41	135.9	90.0	29.4	20.3	86.8	68.6	15.0	142.9	453.0	0.602
42	129.4	62.3	21.2	18.8	100.0	69.2	28.3	104.7	404.5	0.517
43	150.0	59.8	24.0	15.0	99.2	56.3	20.1	121.7	396.1	0.514
44	120.0	63.3	15.3	24.8	94.0	40.0	29.7	127.6	394.8	0.469
45	121.2	55.6	28.7	15.1	99.7	52.5	17.6	128.9	398.2	0.422
46	126.9	40.0	15.0	24.8	80.0	83.1	27.8	48.9	319.5	0.287
47	135.1	40.0	29.9	20.9	90.5	85.5	24.8	70.9	362.5	0.308
48	120.0	84.3	25.8	15.0	92.4	87.6	23.1	106.7	434.9	0.533
49	120.0	69.7	20.1	15.0	86.6	79.5	25.9	86.0	382.7	0.549
50	120.0	75.6	25.4	21.6	80.0	69.0	26.2	107.4	405.1	0.564
51	121.0	63.1	28.7	28.1	80.0	40.0	23.2	136.7	399.8	0.485
52	120.0	40.0	26.2	28.8	90.1	84.8	19.4	80.9	370.2	0.262
53	128.1	40.0	30.0	19.4	80.0	68.1	16.6	84.7	338.7	0.263
54	120.0	45.5	15.0	15.0	100.0	78.2	15.0	82.3	351.0	0.237
55	130.6	70.9	15.0	15.0	80.0	88.5	15.0	77.4	361.8	0.452
56	131.9	40.0	19.5	30.0	93.4	85.8	27.8	69.2	365.7	0.163
57	150.0	64.1	28.1	23.5	80.1	40.0	15.0	140.8	391.6	0.471
58	136.5	64.6	15.0	30.0	80.0	69.9	15.0	104.7	379.2	0.290
59	142.3	52.6	23.0	27.2	80.3	90.0	17.7	75.4	366.2	0.328
60	123.1	40.0	19.8	30.0	94.9	40.0	19.9	124.8	369.4	0.120

Table S3. *Summary of the experimental conditions automatically selected by the decision-making policies utilized in autonomous optimization campaigns.*

Exp. #	Temp. (°C)	CuI ($\mu L.min^{-1}$)	OA_{CuI} ($\mu L.min^{-1}$)	OAm_{CuI} ($\mu L.min^{-1}$)	ODE_{CuI} ($\mu L.min^{-1}$)	CsOleate ($\mu L.min^{-1}$)	$OA_{CsOleate}$ ($\mu L.min^{-1}$)	$ODE_{CsOleate}$ ($\mu L.min^{-1}$)	PFO ($\mu L.min^{-1}$)	Normalized PL_I
EI-1	148.9	90.0	25.7	26.2	99.5	85.8	28.4	127.2	482.8	0.597
EI-2	146.6	77.1	21.1	15.7	80.1	43.2	29.8	121.1	388.1	0.606
EI-3	135.6	89.1	15.0	27.9	97.6	43.3	25.6	160.6	459.0	0.552
EI-4	138.6	90.0	20.3	27.6	89.1	40.0	15.0	172.1	454.1	0.588
EI-5	147.0	85.1	27.5	16.1	85.0	69.2	29.6	114.9	427.5	0.598
EI-6	144.2	90.0	15.0	15.0	86.6	40.0	29.9	136.7	413.2	0.657
EI-7	130.9	60.2	17.5	15.2	99.0	89.7	15.0	87.1	383.7	0.531
EI-8	140.1	90.0	15.0	22.1	89.9	77.9	26.5	112.6	434.0	0.644
EI-9	147.8	90.0	27.7	15.0	86.6	53.5	30.0	135.8	438.6	0.591
EI-10	132.9	73.8	17.3	15.0	99.1	87.5	19.8	97.9	410.5	0.575
EPLT-1	150.0	90.0	19.1	20.1	94.1	58.2	29.5	135.5	446.4	0.632
EPLT-2	150.0	90.0	15.0	27.7	93.2	90.0	23.3	112.6	451.7	0.649
EPLT-3	120.0	90.0	30.0	22.9	92.8	63.0	21.3	151.4	471.5	0.584
EPLT-4	134.8	90.0	27.0	28.9	96.8	40.0	28.6	174.2	485.6	0.579
EPLT-5	122.5	66.2	29.7	25.7	80.0	76.3	27.8	97.5	403.1	0.528
EPLT-6	136.5	84.4	30.0	21.4	92.4	73.4	22.8	132.0	456.5	0.592
EPLT-7	150.0	82.2	23.2	24.0	80.0	66.8	15.0	127.7	418.9	0.651
EPLT-8	120.0	90.0	29.3	28.2	92.9	40.0	21.3	179.1	480.7	0.568
EPLT-9	136.0	90.0	29.3	27.4	92.5	55.7	24.6	158.9	478.4	0.602
EPLT-10	150.0	90.0	15.0	30.0	99.0	90.0	15.0	129.0	468.0	0.658
UCB-1	139.9	90.0	22.8	18.9	80.0	87.3	30.0	94.5	423.5	0.621
UCB-2	133.8	90.0	16.9	19.3	100.0	40.0	15.6	170.6	452.4	0.610
UCB-3	133.5	81.8	24.6	15.0	100.0	90.0	26.4	105.0	442.8	0.604
UCB-4	128.6	55.3	30.0	15.0	80.0	56.1	19.1	105.1	360.6	0.519
UCB-5	124.8	77.8	17.9	26.9	94.9	89.0	26.4	102.2	435.0	0.637
UCB-6	142.3	90.0	15.0	22.6	95.1	86.4	15.0	121.3	445.4	0.613
UCB-7	120.0	55.0	15.0	19.5	91.0	40.0	20.1	120.4	361.0	0.530
UCB-8	147.5	90.0	15.0	23.4	94.2	56.3	29.1	137.2	445.1	0.649
UCB-9	143.3	62.6	28.8	24.6	80.0	53.0	15.0	127.9	391.9	0.541
UCB-10	136.7	70.1	24.3	23.4	97.2	40.0	30.0	145.0	430.0	0.540
Random-1	120.3	47.2	17.2	29.4	86.3	88.0	16.6	75.5	360.2	0.277
Random-2	120.5	41.4	28.8	23.4	87.6	40.7	22.6	117.8	362.3	0.205
Random-3	127.9	68.3	24.5	26.5	91.9	65.8	18.5	126.8	422.2	0.502
Random-4	128.4	51.5	18.5	16.2	97.7	70.4	22.0	91.6	368.0	0.523
Random-5	128.9	41.0	26.9	25.8	90.2	85.5	15.2	83.1	367.7	0.352
Random-6	126.0	49.7	21.7	27.1	82.8	69.0	22.2	90.2	362.6	0.447
Random-7	130.6	48.1	19.0	19.0	92.4	46.7	20.1	111.6	356.8	0.487
Random-8	127.9	44.6	15.5	20.0	90.0	86.7	20.5	62.9	340.3	0.478

Random-9	138.2	57.4	19.4	26.1	85.2	59.5	18.8	109.8	376.3	0.493
Random-10	139.9	54.2	29.8	18.3	87.3	68.8	28.9	92.0	379.5	0.519

S10. Supplementary Movie

Movie M1. A video of the segmented flow format synthesizing $Cs_3Cu_2I_5$ NCs in the SDFL reactor under UV illumination.

References:

1 R. W. Epps, M. S. Bowen, A. A. Volk, K. Abdel-Latif, S. Han, K. G. Reyes, A. Amassian and M. Abolhasani, *Adv. Mater.*, 2020, **32**, 2001626.